The Astronomical Journal, 139:1579–1591, 2010 April doi:10.1088/0004-6256/139/4/1579

NEW PRECISION ORBITS OF BRIGHT DOUBLE-LINED SPECTROSCOPIC BINARIES. IV. 66 ANDROMEDAE, HR 6979, AND HR 9059

Francis C. Fekel[1,3], Jocelyn Tomkin[2], and Michael H. Williamson[1]
[1] Center of Excellence in Information Systems, Tennessee State University, 3500 John A. Merritt Boulevard, Box 9501, Nashville, TN 37209, USA; fekel@evans.tsuniv.edu
[2] Astronomy Department and McDonald Observatory, University of Texas, Austin, TX 78712, USA; jt@alexis.as.utexas.edu
Received 2010 January 21; accepted 2010 February 6; published 2010 March 11

ABSTRACT

We have determined improved spectroscopic orbits for three double-lined binaries, 66 And (F4 V), HR 6979 (Am), and HR 9059 (F5 IV) using radial velocities from the 2.1 m telescope at McDonald Observatory, the coudé feed telescope at Kitt Peak National Observatory, and 2 m telescope at Fairborn Observatory. The orbital periods range from 11.0 to 14.3 days, and all three systems have eccentric orbits. The new orbital dimensions ($a_1 \sin i$ and $a_2 \sin i$) and minimum masses ($m_1 \sin^3 i$ and $m_2 \sin^3 i$) have accuracies of 0.2% or better. All six components of the three binary systems are rotating more slowly than their predicted pseudosynchronous rotational velocities. *Hipparcos* photometry of HR 9059 shows that this system has partial eclipses. Its components are nearly identical in mass and are at the very end of their main-sequence lifetimes or perhaps have just begun to traverse the Hertsprung gap.

Key words: binaries: eclipsing – binaries: spectroscopic – stars: individual (66 And, HR 6979, HR 9059)

1. INTRODUCTION

Three-dimensional orbits can be determined for binary stars that are resolved as both a spectroscopic and a visual binary. This leads to the direct determination of the components' stellar masses. The measured angular and linear separations produce a precise "orbital parallax" of the system. In recent years, major improvements in ground-based optical and near-infrared interferometry have resulted in an increased overlap of spectroscopic and visual binary domains (Quirrenbach 2001). Cunha et al. (2007) produced a list of more than 30 interferometric visual orbits for double-lined spectroscopic binaries, while Torres et al. (2009) identified 23 interferometric systems with stellar masses determined to better than 3%. Work on individual systems (e.g., Hummel et al. 2001; Boden et al. 2006; Fekel et al. 2009a) has led to useful comparisons with evolutionary theory.

Many of the older spectroscopic orbits given in SB9, the web-based edition of the spectroscopic binary orbit catalog (Pourbaix et al. 2004), were computed with radial velocities from photographic plates, which limit the precision of three-dimensional orbits. Thus, in this series of papers (Tomkin & Fekel 2006, 2008; Fekel et al. 2009b) we have obtained additional radial velocities and computed new spectroscopic orbits for bright field spectroscopic binaries, which are the most accessible systems to interferometry. These improved spectroscopic orbits will complement prospective interferometric observations. The three stars, 66 And, HR 6979, and HR 9059, that are analyzed in this paper have been grouped together because of their similar orbital periods, and Table 1 gives some of their basic properties. One of the three systems, HR 9059, has been found to be an eclipsing binary.

[3] Visiting Astronomer, Kitt Peak National Observatory, National Optical Astronomy Observatory, operated by the Association of Universities for Research in Astronomy, Inc. under cooperative agreement with the National Science Foundation.

2. BRIEF HISTORY

2.1. 66 And = HR 709 = HD 15138

The star 66 And [$\alpha = 02^h27^m51\overset{s}{.}78$, $\delta = 50°34'11\overset{''}{.}9$ (2000)] was part of a radial velocity survey of 681 objects that was carried out at the David Dunlap Observatory (DDO). From four DDO spectrograms, Young (1945) reported the velocity variability of this double-lined spectroscopic binary and stated that the components are about equal in line strength. He also listed a spectral class of F2 for the combined spectrum. Over a decade later in a DDO yearly report (Heard 1956), the work of R. J. Northcott on this star was highlighted. A second report, two years later (Heard 1958), stated that she had prepared the orbit of 66 And for publication. Although an analysis of the orbit was never published, R. J. Northcott (1965, private communication) supplied her orbital elements for the sixth edition catalog of spectroscopic binary orbital elements (Batten 1967). That orbit has a period of 10.9903 days and an eccentricity of 0.184. Abt & Levy (1969) reported that an earlier series of plates, 25 of which showed double lines, had been obtained at Mount Wilson between 1932 and 1936 (Abt 1970). However, Abt & Levy (1969) were unsuccessful in determining an orbit from them, and so they acquired 15 coudé spectrograms at the Kitt Peak National Observatory (KPNO). Confirming the description of Young (1945), they noted that the lines of the two components were essentially indistinguishable. They analyzed their new radial velocities and obtained an orbital period of 9.3737 days and an eccentricity of 0.10. In the seventh edition of the binary orbits catalog, Batten et al. (1978) examined the two different orbital solutions and concluded that the 11 day period of Northcott is the correct one.

Appenzeller (1967), Abt & Levy (1969), and Cowley (1976) are in complete agreement that the combined spectrum of 66 And has a spectral type of F4 V. In addition to determining an orbit and spectral type for 66 And, Abt & Levy (1969) also estimated a $v \sin i$ upper limit of 10 km s^{-1} for each component.

Table 1
Basic Properties of the Program Stars

Name	HR	HD	Spectral Type	V^a	$B-V^a$	Parallax[b] (mas)	Period (days)
66 And	709	15138	F4 V	6.16	0.435	17.69	10.99
...	6979	171653	Am	6.60	0.341	7.59	14.34
...	9059	224355	F5 IV	5.57	0.478	14.09	12.16

Notes.
[a] Perryman et al. (1997).
[b] van Leeuwen (2007).

2.2. HR 6979 = HD 171653

The binary nature of HR 6979 [$\alpha = 18^h31^m14^s.90$, $\delta = 65^\circ26'09''.7$ (2000)] was discovered at the Dominion Astrophysical Observatory (DAO) in 1926. Shortly thereafter, Petrie (1928) determined an orbit, based on radial velocity measurements of 26 double-lined photographic plates that were obtained over a 15 month time span. In the intervening four score years no additional orbits have been published. Cowley et al. (1969) characterized the spectrum of HR 6979 as mildly metallic lined, A8m:, where the given spectral class referred to the Ca K line of the combined spectrum. Stickland (1973) included HR 6979 in his abundance analysis of seven double-lined, metallic-lined A stars and confirmed the overabundance of iron, which is a hallmark of Am stars, in both components. More recently, Abt & Morrell (1995) classified the composite spectrum as that of a classical Am star.

2.3. HR 9059 = HD 224355 = V1022 Cas

Plaskett et al. (1920) provided a list of the first 100 spectroscopic binaries discovered at the DAO. The final star in that enumeration was HR 9059 [$\alpha = 23^h57^m08^s.47$, $\delta = 55^\circ42'20''.5$ (2000)], which was found to be a double-lined binary in 1919 by H. H. Plaskett. Harper (1923) analyzed 30 spectrograms and obtained the first orbit of the system. He determined a moderately eccentric orbit with a period of 12.155 days. From that orbit he computed relatively large minimum masses of 1.7 $M_\odot$ for the two F-type components. Over a decade later, Harper (1935) used four additional observations to revise the orbital period to 12.1565 days. That remained the ultimate word on the orbit of HR 9059 until Imbert (1977) recomputed the binary elements with the help of 18 spectrograms obtained at Haute-Provence Observatory (HPO). Using *Hipparcos* photometry (Perryman et al. 1997), Otero (2006) concluded that HR 9059 is an EA-type eclipsing binary.

In a survey of lithium abundances in F stars, Balachandran (1990) observed HR 9059 at a phase when the component lines were blended. For the combined spectrum she determined a low lithium abundance and solar iron abundance.

In their discovery paper, Plaskett et al. (1920) gave the combined spectral class of this double-lined binary as F5. Similar types have been found by most others. Abt & Bidelman (1969) reported that W. W. Morgan classified the composite system as F5 IVn, while Cowley (1976) gave it a spectral type of F6 V. However, from objective prism plates Yoss (1961) estimated an extremely different type of G8 Ib.

3. OBSERVATIONS AND RADIAL VELOCITIES

From 2004 to 2007 we acquired observations at McDonald Observatory with the 2.1 m telescope, the Sandiford Cassegrain echelle spectrograph (McCarthy et al. 1993), and a Reticon CCD. The spectrograms cover the wavelength range 5700–7000 Å and have a resolving power of 49,000.

From 2004 through 2009 we obtained spectrograms at KPNO with the coudé feed telescope and coudé spectrograph. Nearly all were made with a TI CCD detector, and those spectrograms are centered at 6430 Å, cover a wavelength range of 84 Å, and have a resolution of 0.21 Å or a resolving power of just over 30,000. The TI CCD was unavailable in 2008 September, and so a Tektronics CCD, designated T1KA, was used instead. With that CCD the spectrum was centered at 6400 Å. Although the wavelength range covered by the chip increased to 172 Å, the trade-off was that the resolving power decreased to 19,000. Further details about our observations and data reduction are given in Tomkin & Fekel (2006).

Finally, from 2003 through 2009, we collected additional observations with the Tennessee State University 2 m automatic spectroscopic telescope (AST), a fiber-fed echelle spectrograph, and a 2048 × 4096 SITe ST-002A CCD. The echelle spectrograms have 21 orders that cover the wavelength range 4920–7100 Å with an average resolution of 0.17 Å. The typical signal-to-noise ratio of these observations is ∼30. Eaton & Williamson (2004, 2007) have given a more extensive description of the telescope and spectrograph, operated at Fairborn Observatory near Washington Camp in the Patagonia Mountains of southeastern Arizona.

The spectra of the three systems are double-lined and, at most orbital phases, the secondary lines are well separated from their primary counterparts. The procedures used to measure the McDonald and KPNO radial velocities have been described in Tomkin & Fekel (2006). Here we note that the McDonald velocities are absolute velocities, which were placed on a secure rest scale by means of the telluric O_2 and H_2O lines in the stellar spectra.

The KPNO velocities were determined by cross correlation with respect to IAU radial velocity standard stars of the same or similar spectral type as the program stars. The velocities adopted for those standards are from Scarfe et al. (1990). A comparison of the McDonald and KPNO velocities by Tomkin & Fekel (2006) showed that they are consistent with each other to within 0.1–0.2 km s^{-1}, or better. Additional comparisons of data sets from the two observatories have reinforced the conclusion that the velocity zero-point differences are indeed small, and so we have made no adjustment to the velocities.

Fekel et al. (2009b) described the measurement of the radial velocities from the Fairborn Observatory AST spectra. Those velocities, like the ones from McDonald Observatory, are absolute velocities. Our unpublished velocities of several IAU standard solar-type stars indicate that the Fairborn Observatory velocities have a small zero-point offset of −0.3 km s^{-1} relative to the velocities of Scarfe et al. (1990). Thus, we have added 0.3 km s^{-1} to each Fairborn velocity.

4. DETERMINATION OF ORBITS AND RESULTS

We have determined the orbital elements with several computer programs. Preliminary orbits were computed with the program BISP (Wolfe et al. 1967), which implements a slightly modified version of the Wilsing–Russell method. Eccentric orbits were then determined with SB1 (Barker et al. 1967), a program that uses differential corrections. For a simultaneous solution of the two components, we used SB2, which is a slightly modified version of SB1.

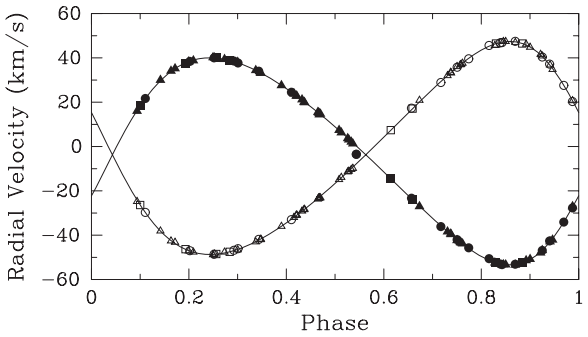

Figure 1. Radial velocities of 66 And compared with the computed velocity curves. Filled and open symbols represent the primary and secondary, respectively. Squares = McDonald Observatory, circles = KPNO, triangles = Fairborn Observatory. Zero phase is a time of periastron passage.

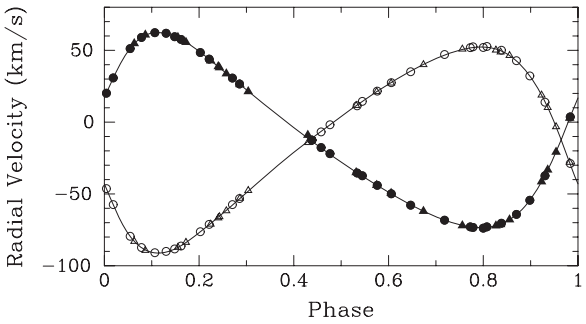

Figure 2. Radial velocities of HR 6979 compared with the computed velocity curves. Filled and open symbols represent the primary and secondary, respectively. Circles = KPNO, triangles = Fairborn Observatory. Zero phase is a time of periastron passage.

The spectra that we obtained at three different observatories have different wavelength ranges. Thus, different numbers of lines were available for measurement. In addition, the primary and secondary lines are of different quality because the components differ to some extent in strength and sometimes in width. Thus, the velocity precision of each set of data will vary from observatory to observatory, and the precision will also usually differ for each primary and secondary component. To determine the weight for each set of our velocities, as well as those from the literature, we computed the variances of the individual orbital solutions, which are inversely proportional to our adopted weights.

4.1. 66 And

We acquired our radial velocities (Table 2) at three observatories, eight from McDonald, 20 from KPNO, and 50 from Fairborn Observatory. We first computed single-lined orbital solutions for both components using the separate data sets. A comparison of those six solutions indicated that the center-of-mass velocities and other elements in common to the individual solutions are in excellent agreement. The McDonald velocities are the most precise, but because of their small number, we have chosen to reduce their relative weighting compared to the Fairborn and KPNO velocities. For the primary our weights are 1.0, 0.6, and 0.4, respectively. For the secondary, the velocity weights are 1.0, 0.4, and 0.4 for McDonald, Fairborn, and KPNO, respectively. The velocities of one KPNO observation, when the components were at a very blended phase, have been given zero weights. A simultaneous solution of the weighted primary and secondary velocities produced a period of 10.98986 days.

We also investigated the possibility of combining our velocities with the earlier photographic ones since they would substantially extend the time baseline and potentially improve the period precision. However, Abt & Levy (1969) reported that the Mount Wilson Observatory velocities from the 1930s are unreliable, and the DDO velocities are mostly unpublished. Thus, we have only examined the KPNO photographic plate velocities of Abt & Levy (1969). They stated that on their 13.4 Å mm^{-1} plates, the lines of the two components are essentially indistinguishable, and Batten et al. (1978) concluded that Abt & Levy (1969) determined the wrong orbital period. Orbital solutions with our elements adopted require the component velocities to be switched except for the ones obtained on JD 2440,197.819. The variance of the solution of the primary velocities produces relative weights that are less than 0.005, and so those velocities do not significantly improve our new orbital solution.

Thus, Table 3 lists the resulting elements from our simultaneous solution of the two components with only our data. Figure 1 compares our new primary and secondary velocities with the calculated velocity curves, and zero phase is a time of periastron passage. Examining the elements of Northcott from Batten et al. (1978) (Table 3) and our new orbital elements, we find that our elements are generally consistent with those of Northcott but are much more precise. The center-of-mass velocities of the two solutions differ by 1.6 km s^{-1}. That modest disagreement is attributed to a combination of the velocity uncertainty of the photographic plate measurements and different observatory zero-points.

4.2. HR 6979

Our new observations were obtained at KPNO and Fairborn Observatory. Nearly all of the 30 KPNO and 23 Fairborn spectrograms were acquired at phases when the components were completely resolved. All the velocities are listed in Table 4. We initially computed four single-lined orbital solutions. The center-of-mass velocities of those four orbits agreed to within 0.1 km s^{-1}, and the corresponding semi-amplitudes were also very consistent. Comparing the variances of the individual solutions, the weights are 1.0 and 0.5 for the primary and secondary velocities, respectively, except for the velocities of two observations, which were given weights of zero, because they were very close to single-lined phases. A simultaneous solution of the appropriately weighted primary and secondary velocities produced a period of 14.36458 days.

The DAO velocities in the literature (Petrie 1928) were obtained about 80 years ago, and so in theory could improve the precision of the period. We analyzed the velocities of the primary component, computing a solution that adopted our orbital elements except for the center-of-mass velocity. The resulting residuals for many of the velocities are so large, up to 20 km s^{-1}, that the velocities are not useful, and so we have not obtained a combined solution. Therefore, we have chosen to list in Table 5 the orbital solution determined with the new velocities from our two observatories. Figure 2 compares our primary and secondary velocities with the calculated velocity curves. Zero phase is a time of periastron passage.

In addition to our elements, Table 5 lists those of Petrie (1928). Despite the fact that the velocities of Petrie (1928) were obtained over a time span of only 15 months, the orbital periods of the two sets of elements are in reasonable agreement, as are the component semiamplitudes. However, our eccentricity of 0.305 is considerably larger than the value of 0.21 from Petrie (1928). Because of our increased eccentricity, our minimum masses are

Table 2
Radial Velocities of 66 And

Hel. Julian Date (HJD − 2,400,000)	Phase	V_1 (km s^{-1})	$(O-C)_1$ (km s^{-1})	Wt_1	V_2 (km s^{-1})	$(O-C)_2$ (km s^{-1})	Wt_2	Source[a]
52,968.804	0.470	14.7	0.3	0.6	−23.1	−0.7	0.4	Fair
53,034.714	0.467	15.0	0.1	0.6	−23.1	−0.2	0.4	Fair
53,037.823	0.750	−42.3	−0.3	0.6	36.1	0.4	0.4	Fair
53,313.884	0.870	−53.4	−0.2	0.6	47.0	−0.3	0.4	Fair
53,319.947	0.422	22.8	0.0	0.6	−30.9	0.1	0.4	Fair
53,330.923	0.420	22.9	−0.1	0.6	−31.0	0.2	0.4	Fair
53,341.000	0.337	34.4	0.0	0.6	−43.0	−0.1	0.4	Fair
53,352.851	0.416	23.9	0.2	0.6	−32.0	−0.1	0.4	Fair
53,353.868	0.508	7.4	0.1	0.6	−14.9	0.1	0.4	Fair
53,386.887	0.513	6.3	−0.1	0.6	−13.9	0.2	0.4	Fair
53,404.789	0.142	30.0	0.2	0.6	−38.1	0.0	0.4	Fair
53,639.994	0.544	−3.5	−3.8	0.0	−3.5	4.3	0.0	KPNO
53,662.749	0.614	−14.3	0.1	1.0	7.4	0.1	1.0	McD
53,691.783	0.256	40.0	0.1	1.0	−48.5	0.1	1.0	McD
53,775.613	0.884	−52.5	0.0	1.0	46.5	0.0	1.0	McD
53,911.979	0.292	38.6	0.3	0.4	−46.8	0.2	0.4	KPNO
54,004.933	0.750	−42.0	0.1	0.4	35.8	0.0	0.4	KPNO
54,005.946	0.843	−53.3	−0.2	0.4	46.9	−0.2	0.4	KPNO
54,007.018	0.940	−42.6	0.6	0.4	37.2	0.3	0.4	KPNO
54,047.887	0.659	−23.9	0.0	1.0	17.1	0.0	1.0	McD
54,049.767	0.830	−52.3	0.1	1.0	46.5	0.1	1.0	McD
54,107.683	0.100	18.3	0.0	1.0	−26.4	0.0	1.0	McD
54,108.706	0.193	37.6	−0.2	1.0	−46.3	0.1	1.0	McD
54,109.701	0.284	38.8	0.0	1.0	−47.5	0.0	1.0	McD
54,367.860	0.774	−45.7	0.3	0.4	39.6	−0.2	0.4	KPNO
54,368.908	0.870	−53.1	0.2	0.4	47.5	0.2	0.4	KPNO
54,370.004	0.969	−34.1	0.0	0.4	27.6	0.0	0.4	KPNO
54,407.819	0.410	24.5	−0.1	0.4	−33.0	−0.2	0.4	KPNO
54,729.897	0.717	−36.1	−0.3	0.4	28.9	−0.5	0.4	KPNO
54,730.983	0.816	−50.6	0.7	0.4	45.6	0.4	0.4	KPNO
54,732.864	0.987	−27.7	−0.2	0.4	20.3	−0.5	0.4	KPNO
54,845.647	0.250	40.2	0.2	0.6	−48.8	−0.1	0.4	Fair
54,847.711	0.437	19.9	−0.3	0.6	−28.3	0.0	0.4	Fair
54,857.706	0.347	33.2	−0.1	0.6	−42.0	−0.2	0.4	Fair
54,859.675	0.526	3.7	−0.1	0.6	−11.4	0.0	0.4	Fair
54,863.786	0.900	−50.8	0.1	0.6	44.8	−0.1	0.4	Fair
54,867.661	0.253	40.1	0.1	0.6	−48.5	0.1	0.4	Fair
54,869.634	0.432	21.2	0.2	0.6	−29.1	0.1	0.4	Fair
54,875.736	0.987	−27.0	0.4	0.6	20.7	0.1	0.4	Fair
54,877.759	0.172	35.2	0.0	0.6	−43.2	0.5	0.4	Fair
54,881.734	0.533	2.1	−0.3	0.6	−10.3	−0.4	0.4	Fair
54,888.659	0.163	34.1	0.2	0.6	−42.6	−0.2	0.4	Fair
54,892.759	0.536	1.3	−0.4	0.6	−9.8	−0.5	0.4	Fair
54,903.657	0.528	3.1	−0.3	0.6	−11.1	−0.1	0.4	Fair
54,907.657	0.892	−51.4	0.4	0.6	46.2	0.4	0.4	Fair
54,911.609	0.252	40.0	0.0	0.4	−48.6	0.1	0.4	KPNO
54,912.616	0.343	34.0	0.3	0.4	−41.9	0.3	0.4	KPNO
54,923.656	0.348	33.2	0.0	0.6	−41.8	−0.1	0.4	Fair
54,924.627	0.436	20.1	−0.3	0.6	−28.5	0.0	0.4	Fair
54,962.971	0.925	−46.8	−0.1	0.6	40.9	0.3	0.4	Fair
54,979.923	0.468	14.4	−0.5	0.6	−23.1	−0.3	0.4	Fair
54,993.883	0.738	−39.6	0.2	0.6	33.2	−0.2	0.4	Fair
55,003.981	0.657	−23.3	0.1	0.4	17.3	0.7	0.4	KPNO
55,006.892	0.922	−47.9	−0.5	0.6	41.6	0.3	0.4	Fair
55,023.866	0.466	15.3	0.2	0.6	−23.3	−0.2	0.4	Fair
55,031.927	0.200	38.3	0.0	0.6	−47.1	−0.1	0.4	Fair
55,052.740	0.094	16.0	−0.2	0.6	−24.8	−0.6	0.4	Fair
55,070.732	0.731	−38.4	0.0	0.6	32.0	0.0	0.4	Fair
55,076.693	0.273	39.4	0.0	0.6	−47.6	0.4	0.4	Fair
55,088.966	0.390	27.6	0.0	0.6	−36.0	0.0	0.4	Fair
55,089.790	0.465	15.5	0.1	0.6	−23.7	−0.4	0.4	Fair
55,092.783	0.737	−39.4	0.3	0.6	33.5	0.2	0.4	Fair
55,093.899	0.839	−53.0	−0.1	0.4	46.8	−0.1	0.4	KPNO
55,093.970	0.845	−53.2	0.0	0.6	47.4	0.2	0.4	Fair

Table 2
(Continued)

Hel. Julian Date (HJD − 2,400,000)	Phase	V_1 (km s^{-1})	$(O-C)_1$ (km s^{-1})	Wt_1	V_2 (km s^{-1})	$(O-C)_2$ (km s^{-1})	Wt_2	Source[a]
55,094.848	0.925	−46.9	−0.2	0.4	40.4	−0.2	0.4	KPNO
55,096.886	0.111	21.7	0.0	0.4	−29.7	0.1	0.4	KPNO
55,097.890	0.202	38.4	−0.1	0.4	−47.0	0.1	0.4	KPNO
55,098.978	0.301	37.7	0.0	0.4	−46.1	0.3	0.4	KPNO
55,103.990	0.757	−43.2	0.0	0.6	36.9	0.0	0.4	Fair
55,105.014	0.850	−53.3	0.0	0.6	47.4	0.0	0.4	Fair
55,106.014	0.941	−42.9	0.0	0.6	36.8	0.2	0.4	Fair
55,130.940	0.209	38.8	−0.2	0.6	−47.6	0.1	0.4	Fair
55,131.940	0.300	38.1	0.3	0.6	−46.6	−0.2	0.4	Fair
55,136.039	0.673	−27.0	−0.1	0.6	20.9	0.7	0.4	Fair
55,136.980	0.759	−43.5	0.0	0.6	37.1	−0.1	0.4	Fair
55,137.739	0.828	−52.4	−0.1	0.6	45.6	−0.7	0.4	Fair
55,139.040	0.946	−42.1	−0.6	0.6	34.8	−0.4	0.4	Fair
55,158.989	0.761	−43.8	0.1	0.6	37.6	−0.1	0.4	Fair

Notes. [a] Fair = Fairborn Observatory, KPNO = Kitt Peak National Observatory, McD = McDonald Observatory.

Table 3
Orbital Elements and Related Parameters of 66 And

Parameter	Northcott in Batten et al. (1978)	This Study
P (days)	10.9903	10.989861 ± 0.000024
T (JD)	2,437,005.979	2,454,007.675 ± 0.006
e	0.184	0.19236 ± 0.00057
ω_1 (deg)	271.3	250.55 ± 0.18
K_1 (km s^{-1})	46.5	46.719 ± 0.034
K_2 (km s^{-1})	50.0	48.083 ± 0.038
γ (km s^{-1})	−5.3	−3.705 ± 0.019
$m_1 \sin^3 i$ ($M_\odot$)	0.51	0.4661 ± 0.0008
$m_2 \sin^3 i$ ($M_\odot$)	0.47	0.4529 ± 0.0007
$a_1 \sin i$ (10^6 km)	6.91	6.9283 ± 0.0051
$a_2 \sin i$ (10^6 km)	7.43	7.1306 ± 0.0056
rms residual (km s^{-1}) (unit weight)	...	0.1

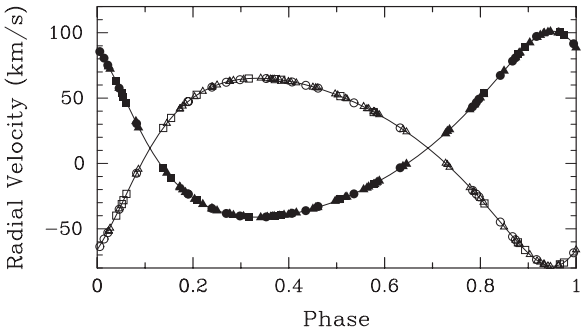

Figure 3. Radial velocities of HR 9059 compared with the computed velocity curves. Filled and open symbols represent the primary and secondary, respectively. Squares = McDonald Observatory, circles = KPNO, and triangles = Fairborn Observatory. Zero phase is a time of periastron passage.

nearly 0.2 $M_\odot$ smaller than those determined by Petrie (1928), but even so, at 1.8 and 1.7 $M_\odot$, they are still rather large. The center-of-mass velocity for the older orbit is about 2 km s^{-1} more positive than ours. This difference is likely caused by the large velocity uncertainty of the photographic plate measurements and different observatory zero points rather than being a sign of a third body in the system.

4.3. HR 9059

We obtained our spectrograms of HR 9059 at three observatories, 17 from McDonald, 24 from KPNO, and 69 from Fairborn. The velocity measurements are given in Table 6. We first computed six separate single-lined orbital solutions, three for each component. From a comparison of those individual solutions, we assigned weights of 0.7, 0.4, and 0.1 for the McDonald, Fairborn, and KPNO radial velocities of the primary, respectively. Similarly, the weights for the secondary velocities from the three observatories were 1.0, 0.3, and 0.3, respectively. A simultaneous solution of the appropriately weighted primary and secondary velocities resulted in a period of 12.15617 days. The HPO velocities (Imbert 1977) were obtained in 1961, and so would extensively extend the time span of the data. We, thus, computed an orbit for the HPO data alone, fixing the period at the value determined by Imbert (1977) from the combined solution of his and Harper's data. The systemic velocity of that solution differs from ours by 2 km s^{-1}, and the velocity weights are extremely small, 0.002, relative to those of our McDonald observations. Thus, the inclusion of the HPO velocities with those from our three observatories, does not significantly improve the orbital solution, and so, we have chosen to list in Table 7 our orbital solution, determined with the velocities from just our three observatories.

Figure 3 is a plot of our new primary and secondary velocities and the calculated velocity curves, where zero phase is a time of periastron passage. A comparison of the two orbital solutions in Table 7 shows that our orbital elements are generally consistent with those of Imbert (1977) but much more precise. The orbital periods of the two sets of elements are nearly identical to within their uncertainties. On the other hand, our center-of-mass velocity agrees with the value of 11.98 ± 0.32 found by Harper (1923), but is 2 km s^{-1} higher than the value from the HPO velocities. This difference results from either different observatory velocity zero points, or the influence of a third body. Although the latter possibility cannot be completely ruled out, our very precise velocities from 2004 through 2009 show no evidence of third-body effects, and the center-of-mass velocity difference is small enough to result from observatory

Table 4
Radial Velocities of HR 6979

Hel. Julian Date (HJD − 2,400,000)	Phase	V_1 (km s^{-1})	$(O-C)_1$ (km s^{-1})	Wt_1	V_2 (km s^{-1})	$(O-C)_2$ (km s^{-1})	Wt_2	Source[a]
53,276.869	0.674	−62.0	−0.1	1.0	40.1	−0.1	0.5	Fair
53,313.774	0.243	38.0	−0.2	1.0	−65.8	−0.3	0.5	Fair
53,488.954	0.438	−12.5	0.8	0.0	−12.5	−1.3	0.0	KPNO
53,490.935	0.576	−44.0	0.1	1.0	21.6	0.2	0.5	KPNO
53,491.949	0.647	−57.8	−0.4	1.0	35.1	−0.4	0.5	KPNO
53,492.976	0.718	−68.3	−0.1	1.0	47.1	0.3	0.5	KPNO
53,536.853	0.773	−72.9	0.0	1.0	51.9	0.1	0.5	KPNO
53,639.668	0.930	−37.3	−0.1	1.0	13.9	−0.2	0.5	KPNO
53,852.955	0.778	−73.3	−0.1	1.0	52.5	0.5	0.5	KPNO
53,855.904	0.984	3.7	0.2	1.0	−28.8	0.1	0.5	KPNO
53,856.919	0.054	51.2	0.0	1.0	−79.5	−0.2	0.5	KPNO
53,915.920	0.162	57.6	0.1	1.0	−86.3	−0.4	0.5	KPNO
54,001.656	0.130	61.9	0.1	1.0	−90.0	0.4	0.5	KPNO
54,002.694	0.203	48.5	−0.1	1.0	−76.3	0.2	0.5	KPNO
54,003.666	0.270	30.7	0.0	1.0	−57.4	0.2	0.5	KPNO
54,006.626	0.476	−21.9	0.4	1.0	−1.8	−0.2	0.5	KPNO
54,222.920	0.534	−35.4	−0.2	1.0	11.4	−0.6	0.5	KPNO
54,223.954	0.606	−49.9	0.0	1.0	27.5	0.0	0.5	KPNO
54,269.840	0.800	−73.8	−0.4	1.0	52.0	−0.3	0.5	KPNO
54,366.721	0.545	−37.3	0.2	1.0	14.5	0.1	0.5	KPNO
54,408.565	0.458	−17.7	0.2	1.0	−6.8	−0.5	0.5	KPNO
54,585.970	0.808	−72.9	0.3	1.0	52.7	0.6	0.5	KPNO
54,586.864	0.870	−64.2	0.2	1.0	42.8	0.0	0.5	KPNO
54,643.868	0.838	−70.4	0.4	1.0	50.1	0.6	0.5	KPNO
54,732.646	0.019	30.8	−0.2	1.0	−57.4	0.5	0.5	KPNO
54,847.043	0.983	2.9	0.3	1.0	−28.0	−0.1	0.5	Fair
54,863.890	0.155	59.1	0.5	1.0	−87.2	−0.1	0.5	Fair
54,876.930	0.063	54.8	0.2	1.0	−83.0	−0.2	0.5	Fair
54,903.835	0.936	−33.2	0.1	1.0	10.2	0.2	0.5	Fair
54,927.814	0.605	−49.5	0.4	1.0	27.2	−0.3	0.5	Fair
54,945.771	0.856	−67.9	0.0	1.0	46.4	−0.1	0.5	Fair
54,947.908	0.004	20.2	−0.1	1.0	50.2	−0.7	0.5	KPNO
54,948.971	0.078	59.0	0.1	1.0	−46.3	0.3	0.5	KPNO
54,949.978	0.148	59.5	−0.2	1.0	−87.3	0.1	0.5	KPNO
54,959.721	0.827	−72.1	0.0	1.0	−88.3	−0.1	0.5	Fair
54,984.834	0.575	−43.9	−0.1	1.0	21.3	0.2	0.5	Fair
55,003.842	0.898	−54.4	0.0	1.0	32.2	−0.1	0.5	KPNO
55,006.835	0.107	62.3	−0.2	1.0	−90.9	0.2	0.5	KPNO
55,025.838	0.429	−9.0	2.2	0.0	−14.2	−0.8	0.0	Fair
55,051.853	0.241	38.8	0.0	1.0	−66.7	−0.5	0.5	Fair
55,066.872	0.286	26.3	−0.1	1.0	−53.0	0.0	0.5	Fair
55,080.826	0.257	33.8	−0.4	1.0	−61.7	−0.4	0.5	Fair
55,092.735	0.087	60.8	0.3	1.0	−89.3	−0.2	0.5	Fair
55,094.670	0.221	43.9	0.0	1.0	−71.2	0.3	0.5	KPNO
55,094.716	0.224	42.8	−0.3	1.0	−71.0	−0.3	0.5	Fair
55,095.593	0.286	26.6	0.1	1.0	−53.2	0.0	0.5	KPNO
55,095.855	0.304	21.4	−0.1	1.0	−47.6	0.3	0.5	Fair
55,104.752	0.923	−41.4	0.2	1.0	18.9	0.2	0.5	Fair
55,116.714	0.756	−72.0	−0.1	1.0	50.9	0.2	0.5	Fair
55,122.695	0.172	55.7	0.2	1.0	−83.7	0.1	0.5	Fair
55,146.603	0.837	−71.2	−0.2	1.0	48.9	−0.9	0.5	Fair
55,156.586	0.532	−35.0	−0.3	1.0	11.6	0.1	0.5	Fair
55,162.651	0.954	−20.8	−0.2	1.0	−3.2	0.2	0.5	Fair

Notes. [a] Fair = Fairborn Observatory, KPNO = Kitt Peak National Observatory.

zero-point differences. Our mass ratio of the components is 1.011, the same value as that determined by Imbert (1977). Thus, the components have nearly equal masses. However, our identification of the more massive primary is the *reverse* of that found by Imbert (1977) but the same as that of Harper (1923).

5. SPECTRAL TYPES AND MAGNITUDE DIFFERENCE

Strassmeier & Fekel (1990) identified several luminosity-sensitive and temperature-sensitive line ratios in the 6430–6465 Å region. They employed those critical line ratios and the general appearance of the spectrum as spectral-type criteria.

Table 5
Orbital Elements and Related Parameters of HR 6979

Parameter	Petrie (1928)	This Study
P (days)	14.3450 ± 0.0074	14.364577 ± 0.000030
T (HJD)	2,424,710.897	2,453,999.7839 ± 0.0038
e	0.210 ± 0.027	0.30517 ± 0.00049
ω (deg)	295.9 ± 7.7	289.14 ± 0.11
K_1 (km s^{-1})	68.29 ± 1.97	68.006 ± 0.043
K_2 (km s^{-1})	72.01 ± 2.02	71.790 ± 0.060
γ (km s^{-1})	−10.34 ± 1.08	−12.252 ± 0.026
$m_1 \sin^3 i$ ($M_\odot$)	1.97	1.8075 ± 0.0031
$m_2 \sin^3 i$ ($M_\odot$)	1.87	1.7122 ± 0.0025
$a_1 \sin i$ (10^6 km)	13.173	12.792 ± 0.008
$a_2 \sin i$ (10^6 km)	13.885	13.504 ± 0.012
rms residual (km s^{-1}) (unit weight)	...	0.2

However, for stars that are hotter than early-G spectral class, the line ratios in that wavelength region have little sensitivity to luminosity. Thus, for the A and F stars of our three systems, we have used the entire 84 Å spectral region of our KPNO observations to estimate just the spectral classes of the individual components. The luminosity class may be determined by computing the absolute visual magnitude with the *Hipparcos* parallax and comparing that magnitude to evolutionary tracks or a table of canonical values for giants and dwarfs.

Spectra of our three binaries were compared with the spectra of a number of A- and F-type stars primarily from the lists of Abt & Morrell (1995) and Fekel (1997). The reference star spectra were obtained at KPNO with the same telescope, spectrograph, and detector as our binary star spectra. To facilitate a comparison, various combinations of the reference-star spectra were rotationally broadened, shifted in radial velocity, appropriately weighted, and added together with a computer program developed by Huenemoerder & Barden (1984) and Barden (1985) in an attempt to reproduce the binary spectra.

That analysis has met with limited success for one of our three star systems, HR 6979, because its components are Am stars. Classical Am stars have spectral classes of A4–F1, determined from their hydrogen lines (Abt & Morrell 1995). Such stars are noted as having peculiar spectra because lines of their metallic elements such as iron and strontium are stronger than expected compared to the hydrogen classification, while elements such as calcium and scandium are weaker (Abt & Morrell 1995). There are no hydrogen lines in our limited 6430 Å wavelength region, and the iron and calcium abundance peculiarities vary from star to star, making it impossible to adequately characterize the combined spectrum of the two components with our limited number of reference spectra.

For the other two systems, we have been able to determine a best spectrum model, which has been used to compute the continuum intensity ratio of the binary components at 6430 Å, a wavelength that is about 0.6 of the way between the central wavelengths of the Johnson V and R bandpasses. Because the two components in both systems have very similar spectral types, this intensity ratio is also the luminosity ratio and, thus, can be converted directly into a magnitude difference.

5.1. 66 And

Appenzeller (1967), Abt & Levy (1969), and Cowley (1976) are in complete agreement that the combined spectrum of 66 And has a spectral type of F4 V. The reference stars θ Cyg [F4 V (Slettebak 1955) and mean [Fe/H] = 0.01 (Taylor 2005)] and Procyon [F5IV-V (Johnson & Morgan 1953) and mean [Fe/H] = −0.04 (Taylor 2005)] produce an excellent fit to the primary and secondary, respectively. Thus, the components have nearly solar iron abundances.

The continuum intensity ratio of the secondary/primary is 0.767, which results in a continuum magnitude difference of 0.29 at 6430 Å. The secondary has a similar spectral class to the primary, and so we adopt a V mag difference of 0.3. As discussed in Section 7.1, visual magnitudes from the reanalyzed *Hipparcos* parallax (van Leeuwen 2007) indicate that both components are on the main sequence.

5.2. HR 6979

We are unable to determine spectral classes for the components of HR 6979 because of the Am abundance peculiarities, and the fact that there are no hydrogen lines in our limited 6430 Å wavelength region. We have, however, compared the spectrum of this binary with several reference star spectra and have the following comments.

In his paper on the orbit of HR 6979, Petrie (1928) reported that its spectrum "is characterized by a number of sharp metallic lines." Abt (1975) found v sin i values of 20 km s^{-1} for both components, consistent with that comment, but Abt & Morrell (1995) determined 101 km s^{-1}. This latter much larger value presumably results from an observation that was obtained at a phase when the lines were blended, but unfortunately, this very large value is the one that is currently listed in the "measurements" section of the SIMBAD database. Our spectra show that the lines of both components are even narrower than the values estimated by Abt (1975).

Abt & Morrell (1995) classified the combined spectrum of HR 6979 as A3/F1/F2 for its Ca K, hydrogen, and metals spectral classes, making it a classical Am star. Stickland (1973) carried out an abundance analysis of both components and found them to have very large overabundances of iron. We concur with that result since our comparison of the Fe I lines of HR 6979 with the Fe I lines of HR 5075, an F2 V star with near solar iron abundances (Boesgaard & Tripicco 1986), shows that the lines of HR 6979 are much stronger. For the Ca I lines of HR 6979, we used HR 1613, an A9 V star with normal abundances (Bikmaev et al. 2002), as the comparison star. The Ca I lines of HR 6979 in the 6430 Å region are somewhat weaker for both components, and so we estimate a spectral class of A7 from those calcium lines.

From the equivalent width ratios of several Fe I lines in the 6430 Å region, we adopted a V mag difference of 0.2. The evolutionary track comparison, discussed in Section 7.2, indicates that both components have evolved from the zero age main sequence (ZAMS) but are still dwarfs in the main-sequence band.

5.3. HR 9059

The starting point for our analysis of the spectrum of HR 9059 is the spectral type of F6 V determined by Cowley (1976). We tried several mid- and late-F reference stars but found the best fit when the spectrum of Procyon [F5IV-V (Johnson & Morgan 1953) and mean [Fe/H] = −0.04 (Taylor 2005)] was adopted for both components. Our results are in agreement with those of Balachandran (1990), who analyzed a spectrum of HR 9059 that was obtained when the components were blended. She determined a mean [Fe/H] value of −0.01; so the iron abundances of the components are essentially solar.

Table 6
Radial Velocities of HR 9059

Hel. Julian Date (HJD − 2,400,000)	Phase	V_1 (km s^{-1})	$(O-C)_1$ (km s^{-1})	Wt_1	V_2 (km s^{-1})	$(O-C)_2$ (km s^{-1})	Wt_2	Source[a]
53,170.988	0.842	67.3	−0.4	0.1	−44.8	0.0	0.3	KPNO
53,172.979	0.005	85.6	−0.2	0.1	−63.6	−0.5	0.3	KPNO
53,259.883	0.154	−10.9	0.1	0.7	34.8	0.0	1.0	McD
53,261.854	0.316	−40.8	0.1	0.7	65.0	0.0	1.0	McD
53,273.787	0.298	−40.2	0.0	0.1	64.1	−0.2	0.3	KPNO
53,275.768	0.461	−32.9	0.6	0.1	57.6	0.1	0.3	KPNO
53,277.852	0.633	−3.3	0.4	0.1	27.2	−0.2	0.3	KPNO
53,278.011	0.646	−0.4	0.1	0.4	24.2	0.1	0.3	Fair
53,287.916	0.460	−33.6	0.0	0.4	57.8	0.2	0.3	Fair
53,313.791	0.589	−13.3	0.1	0.4	37.3	0.2	0.3	Fair
53,322.937	0.341	−41.3	−0.2	0.4	65.3	0.2	0.3	Fair
53,341.922	0.903	92.5	0.2	0.4	−69.7	0.0	0.3	Fair
53,342.687	0.966	100.3	0.3	0.7	−77.2	0.3	1.0	McD
53,354.817	0.964	100.2	−0.1	0.4	−77.8	0.0	0.3	Fair
53,360.730	0.450	−34.8	−0.1	0.4	58.4	−0.3	0.3	Fair
53,432.594	0.362	−40.9	−0.2	0.4	64.6	−0.2	0.3	Fair
53,437.647	0.778	41.3	0.0	0.4	−18.5	−0.4	0.3	Fair
53,464.955	0.024	74.4	0.3	0.4	−51.7	−0.4	0.3	Fair
53,478.913	0.172	−17.9	0.1	0.4	41.6	−0.2	0.3	Fair
53,491.901	0.241	−34.7	0.0	0.4	58.6	−0.1	0.3	Fair
53,504.845	0.306	−40.5	0.0	0.4	64.4	−0.2	0.3	Fair
53,528.796	0.276	−38.7	0.1	0.4	62.8	0.0	0.3	Fair
53,531.958	0.536	−23.3	−0.2	0.1	46.4	−0.6	0.3	KPNO
53,534.969	0.784	43.3	−0.3	0.1	−20.6	−0.1	0.3	KPNO
53,535.983	0.867	78.3	−0.2	0.1	−56.0	−0.2	0.3	KPNO
53,536.770	0.932	99.4	−0.1	0.4	−77.1	−0.1	0.3	Fair
53,550.736	0.081	32.2	0.5	0.4	−8.2	0.2	0.3	Fair
53,566.764	0.399	−39.2	−0.2	0.4	62.7	−0.3	0.3	Fair
53,608.997	0.873	81.1	−0.1	0.4	−58.8	−0.4	0.3	Fair
53,613.993	0.284	−39.6	−0.2	0.4	63.6	0.1	0.3	Fair
53,627.011	0.355	−41.0	−0.1	0.4	64.8	−0.1	0.3	Fair
53,634.784	0.995	91.6	0.4	0.1	−68.4	0.2	0.3	KPNO
53,635.847	0.082	30.5	−0.1	0.1	−7.5	−0.2	0.3	KPNO
53,636.952	0.173	−18.4	−0.2	0.4	41.9	−0.2	0.3	Fair
53,637.760	0.240	−34.4	0.1	0.1	58.4	−0.1	0.3	KPNO
53,639.794	0.407	−38.1	0.4	0.1	62.3	−0.2	0.3	KPNO
53,641.931	0.583	−14.8	−0.2	0.4	38.5	0.1	0.3	Fair
53,653.892	0.567	−17.8	−0.1	0.4	41.9	0.3	0.3	Fair
53,661.684	0.208	−27.9	0.4	0.7	52.5	0.3	1.0	McD
53,663.666	0.371	−40.2	0.2	0.7	64.5	0.0	1.0	McD
53,663.830	0.384	−39.6	0.2	0.7	64.0	0.1	1.0	McD
53,669.892	0.883	84.8	−0.1	0.4	−62.1	0.1	0.3	Fair
53,680.876	0.786	44.7	0.0	0.4	−21.5	0.0	0.3	Fair
53,682.819	0.946	100.9	−0.1	0.4	−78.8	−0.3	0.3	Fair
53,689.645	0.508	−27.3	0.2	0.7	51.5	0.1	1.0	McD
53,693.799	0.849	70.8	−0.3	0.4	−48.6	−0.4	0.3	Fair
53,694.912	0.941	100.5	−0.2	0.4	−78.4	−0.2	0.3	Fair
53,721.709	0.145	−7.3	−0.2	0.4	30.7	−0.1	0.3	Fair
53,726.702	0.556	−19.9	−0.2	0.4	43.6	0.1	0.3	Fair
53,734.778	0.221	−31.2	−0.1	0.4	55.2	0.1	0.3	Fair
53,742.805	0.881	84.5	0.4	0.4	−61.7	−0.2	0.3	Fair
53,748.745	0.369	−40.4	0.1	0.4	64.5	0.0	0.3	Fair
53,756.699	0.024	74.1	−0.2	0.4	−51.7	−0.2	0.3	Fair
53,769.614	0.086	27.4	−0.3	0.4	−4.4	0.0	0.3	Fair
53,770.736	0.179	−20.0	0.1	0.4	43.9	0.0	0.3	Fair
53,775.583	0.577	−15.7	0.0	0.7	39.3	−0.2	1.0	McD
53,783.628	0.239	−34.6	−0.2	0.4	58.4	0.0	0.3	Fair
53,797.619	0.390	−39.4	0.1	0.4	63.5	−0.1	0.3	Fair
53,800.638	0.638	−2.2	0.1	0.4	26.0	0.0	0.3	Fair
53,855.898	0.184	−22.0	−0.1	0.4	45.8	0.1	0.3	Fair
53,868.857	0.250	−36.1	−0.1	0.4	60.0	0.0	0.3	Fair
53,871.919	0.502	−28.2	0.1	0.4	52.4	0.1	0.3	Fair
53,884.817	0.563	−18.7	−0.3	0.4	41.9	−0.3	0.3	Fair
53,886.814	0.727	22.9	−0.3	0.4	0.2	0.1	0.3	Fair

Table 6
(Continued)

Hel. Julian Date (HJD − 2,400,000)	Phase	V_1 (km s^{-1})	$(O-C)_1$ (km s^{-1})	Wt_1	V_2 (km s^{-1})	$(O-C)_2$ (km s^{-1})	Wt_2	Source[a]
53,904.754	0.203	−27.3	−0.1	0.4	51.1	0.0	0.3	Fair
53,911.972	0.797	49.2	0.3	0.1	−25.6	0.3	0.3	KPNO
53,996.953	0.788	45.2	0.0	0.4	−22.1	0.0	0.3	Fair
54,001.848	0.190	−23.5	0.3	0.1	47.4	−0.2	0.3	KPNO
54,002.809	0.269	−38.3	−0.1	0.1	62.1	−0.1	0.3	KPNO
54,004.826	0.435	−36.1	0.0	0.1	59.8	−0.4	0.3	KPNO
54,010.880	0.933	99.8	0.0	0.4	−77.0	0.3	0.3	Fair
54,023.843	1.000	88.6	−0.2	0.4	−66.1	0.0	0.3	Fair
54,030.952	0.585	−14.2	0.1	0.4	38.1	0.1	0.3	Fair
54,044.888	0.731	24.7	0.3	0.4	−0.8	0.3	0.3	Fair
54,045.804	0.806	52.9	0.2	0.4	−29.7	0.0	0.3	Fair
54,046.679	0.878	83.5	0.4	0.7	−60.4	0.1	1.0	McD
54,048.640	0.040	62.9	0.1	0.7	−39.9	0.0	1.0	McD
54,048.824	0.055	51.2	0.0	0.7	−28.1	0.1	1.0	McD
54,049.832	0.138	−3.5	−0.1	0.7	27.1	0.0	1.0	McD
54,057.879	0.800	50.3	0.3	0.4	−26.8	0.1	0.3	Fair
54,059.855	0.962	100.1	−0.4	0.4	−77.9	0.1	0.3	Fair
54,072.797	0.027	72.3	0.2	0.4	−49.5	−0.2	0.3	Fair
54,078.769	0.518	−25.8	0.2	0.4	49.9	0.0	0.3	Fair
54,091.643	0.577	−16.0	−0.3	0.4	39.7	0.2	0.3	Fair
54,095.790	0.918	96.6	−0.1	0.4	−74.5	−0.3	0.3	Fair
54,105.723	0.735	26.0	0.1	0.4	−2.9	−0.3	0.3	Fair
54,106.611	0.809	53.6	0.0	0.7	−30.6	0.0	1.0	McD
54,107.643	0.893	89.0	0.1	0.7	−66.2	0.1	1.0	McD
54,108.630	0.975	98.3	0.0	0.7	−75.8	0.0	1.0	McD
54,109.562	0.051	53.9	−0.1	0.7	−31.1	−0.2	1.0	McD
54,109.682	0.061	46.5	0.1	0.7	−23.3	0.0	1.0	McD
54,121.652	0.046	57.7	−0.4	0.4	−34.7	0.5	0.3	Fair
54,136.619	0.277	−38.8	0.1	0.4	62.8	−0.1	0.3	Fair
54,265.961	0.917	97.2	0.8	0.1	−73.6	0.2	0.3	KPNO
54,364.775	0.046	57.6	−0.6	0.1	−35.1	0.1	0.3	KPNO
54,643.984	0.014	80.6	0.1	0.1	−57.8	0.0	0.3	KPNO
54,861.712	0.925	98.2	−0.1	0.4	−75.5	0.3	0.3	Fair
54,869.662	0.579	−15.9	−0.6	0.4	39.6	0.5	0.3	Fair
54,904.006	0.404	−38.5	0.1	0.4	62.4	−0.3	0.3	Fair
54,965.910	0.497	−28.8	0.3	0.4	53.2	0.2	0.3	Fair
55,005.962	0.792	46.6	−0.2	0.1	−23.5	0.1	0.3	KPNO
55,006.953	0.873	80.8	−0.2	0.1	−58.4	−0.1	0.3	KPNO
55,086.978	0.456	−33.8	0.3	0.4	58.0	0.0	0.3	Fair
55,093.856	0.022	75.2	−0.3	0.1	−53.0	−0.3	0.3	KPNO
55,095.887	0.189	−23.2	0.2	0.1	47.4	0.1	0.3	KPNO
55,097.878	0.353	−40.9	0.0	0.1	65.0	0.0	0.3	KPNO
55,099.924	0.521	−25.6	−0.1	0.4	49.5	0.1	0.3	Fair
55,146.836	0.380	−40.1	−0.1	0.4	64.2	0.1	0.3	Fair
55,158.811	0.365	−40.6	0.0	0.4	64.4	−0.3	0.3	Fair
55,183.735	0.416	−37.7	0.1	0.4	61.7	−0.2	0.3	Fair

Notes. [a] KPNO = Kitt Peak National Observatory, McD = McDonald Observatory, Fair = Fairborn Observatory.

The continuum intensity ratio of the secondary/primary is 0.898, which results in a continuum magnitude difference of 0.12 at 6430 Å. The secondary has a similar spectral class to the primary, and so we adopt a *V* mag difference of 0.1. As discussed in Section 7.3, a comparison with evolutionary tracks shows that both stars are at the end of their main-sequence lifetimes or perhaps have just begun their evolution across the Hertzsprung gap. Thus, we classify both components as F5 subgiant/dwarf.

Given the general concordance of the other spectral types noted in Section 2.3 and the color of the combined system (Table 1), all of which indicate that HR9059 is a mid-F dwarf or subgiant, the spectral type of G8 Ib given by Yoss (1961) is most puzzling. Our best guess is that the HD number is a typographical error, although perhaps the star was misidentified when it was observed. Whatever the case, this very discrepant classification found its way into the Bright Star Catalogue (Hoffleit 1982), as well as the *Hipparcos* catalog (Perryman et al. 1997) and is currently in the basic data section of the SIMBAD database. Thus, this discrepancy is an example of the general lack of critical data examination that occurs when large database catalogs are compiled. In their study of the nature of overluminous F stars, Griffin and Suchkov (2003) list in their Table 1 a spectral type of G8 III. That spectral type, which has no attribution, also is clearly at odds with other information, and R. Griffin (2009, private communication) has repudiated it.

Table 7
Orbital Elements and Related Properties of HR 9059

Parameter	Imbert (1977)	This Study
P (days)	12.156153 ± 0.000023	12.156168 ± 0.000012
T (HJD)	2,439,327.11 ± 0.04	2,453,282.3193 ± 0.0014
e	0.312 ± 0.006	0.31167 ± 0.00026
ω (deg)	216.7 ± 1.3	34.453 ± 0.052
K_1 (km s^{-1})	71.75 ± 0.7	71.117 ± 0.027
K_2 (km s^{-1})	72.6 ± 0.7	71.905 ± 0.026
γ (km s^{-1})	10.3 ± 0.3	11.744 ± 0.014
$m_1 \sin^3 i$ ($M_\odot$)	1.637 ± 0.056	1.5930 ± 0.0013
$m_2 \sin^3 i$ ($M_\odot$)	1.618 ± 0.056	1.5755 ± 0.0013
$a_1 \sin i$ (10^6 km)	11.394 ± 0.132	11.296 ± 0.004
$a_2 \sin i$ (10^6 km)	11.528 ± 0.133	11.421 ± 0.004
rms residual (km s^{-1}) (unit weight)	...	0.1

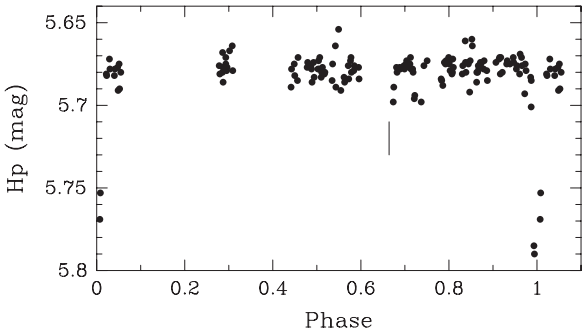

Figure 4. *Hipparcos* H_p magnitudes of HR 9059 phased with our spectroscopically determined ephemeris $T_{\rm conj}$(HJD) = 2,453,283.328(± 0.001) + 12.15617(± 0.00001)E. The partial eclipse of the more massive component is seen at phase 1.0. A tick mark indicates the predicted phase (0.664) of mid-eclipse for the second eclipse.

6. ECLIPSE SEARCHES

6.1. 66 And

With spectral classes of F4 and F5 for the components of 66 And, masses near 1.4 $M_\odot$ are expected (Gray 1992). However, the minimum masses from our orbit are about 0.45 $M_\odot$, or three times smaller. Thus, the orbital inclination is rather low and there is no prospect of eclipses.

6.2. HR 6979

Unlike 66 And, the minimum masses for the components of HR 6979 are large, 1.8 and 1.7 $M_\odot$, suggesting that the components might eclipse. However, because of the eccentricity and orientation of its orbit, an eclipse at the conjunction closer to periastron is more likely. From our orbital elements (Table 5), the separation of the components is smaller for an eclipse when the slightly less massive star is behind the more massive star. The ephemeris for times of mid-eclipse is

$$T_{\rm conj}(HJD) = 2{,}453{,}999.393(\pm 0.004) + 14.36458(\pm 0.00003)E,$$

where E represents an integer number of cycles.

Photometry obtained by *Hipparcos* (Perryman et al. 1997) was plotted with this eclipse ephemeris and shows no evidence of an eclipse at the predicted time. However, no *Hipparcos* observations were obtained within ±0.013 phase units of predicted mid-eclipse phase, so a partial eclipse could still have been present but missed in that interval. Relative to that eclipse, the other eclipse is predicted to occur at phase 0.433. Two points within 0.002 phase units of that phase show no evidence of an eclipse.

6.3. HR 9059

Like HR 6979, the minimum masses of HR 9059 are rather large, in this case nearly 1.6 $M_\odot$, and so eclipses are a possibility. Once again, the eclipse closer to periastron is more likely. From our orbital elements (Table 7), the separation of the components is smaller for the eclipse when the slightly more massive star is behind. Our ephemeris for times of mid-eclipse is

$$T_{\rm conj}(HJD) = 2,453,283.328(\pm 0.001) + 12.15617(\pm 0.00001)E,$$

where E represents an integer number of cycles.

Otero (2006) examined the *Hipparcos* photometry of this system (Perryman et al. 1997) and concluded that HR 9059 is an EA-type eclipsing binary with a secondary eclipse at phase 0.67. We have used our improved eclipse ephemeris to plot the *Hipparcos* photometric data (Perryman et al. 1997). Figure 4 shows a 0.11 mag light decrease at the predicted time, indicating that HR 9059 has partial eclipses. Relative to that eclipse, the mid-eclipse of the slightly less massive secondary occurs at phase 0.664. Although no *Hipparcos* observations were obtained at exactly that phase, Figure 4 shows that there are two low points about 0.01 phase units later that may well be eclipse points.

7. BASIC PROPERTIES

7.1. 66 And

To determine the basic properties of 66 And, we used the Stefan–Boltzmann law. We began by adopting a V mag and $B-V$ color from the *Hipparcos* catalog (Perryman et al. 1997), which are 6.16 and 0.435, respectively. With our V mag difference of 0.3 the apparent V mag of the individual components become 6.77 and 7.07. The new *Hipparcos* parallax reduction by van Leeuwen (2007) results in a value of 17.69 ± 0.42 mas and corresponds to a distance of 56.5 ± 1.3 pc. According to Abt & Levy (1969), the Hβ line strength measured by Crawford et al. (1966) indicates that the system is unreddened. We then combined the apparent magnitudes and the parallax to obtain absolute magnitudes M_V = 3.1 ± 0.1 mag and M_V = 3.4 ± 0.1 mag for the primary and secondary, respectively. We next adopted $B-V$ colors of 0.42 and 0.45 for the primary and secondary, respectively, and then used Table 3 of Flower (1996) to obtain the bolometric corrections and effective temperatures of the two components. The resulting luminosities of the primary and secondary are $L_1 = 4.9 \pm 0.5\,L_\odot$ and $L_2 = 3.8 \pm 0.4\,L_\odot$, respectively, while the radii are $R_1 = 1.7 \pm 0.1\,R_\odot$ and $R_2 = 1.5 \pm 0.1\,R_\odot$, respectively. The uncertainties in the computed quantities are dominated by the parallax uncertainty and the effective temperature uncertainty with the latter estimated to be ± 200 K.

7.2. HR 6979

As we did for 66 And, we used the Stefan–Boltzmann law to determine the basic properties of HR 6979. Our first step again was to adopt a V mag and $B-V$ color for the HR 6979 system. From the *Hipparcos* catalog (Perryman et al. 1997)

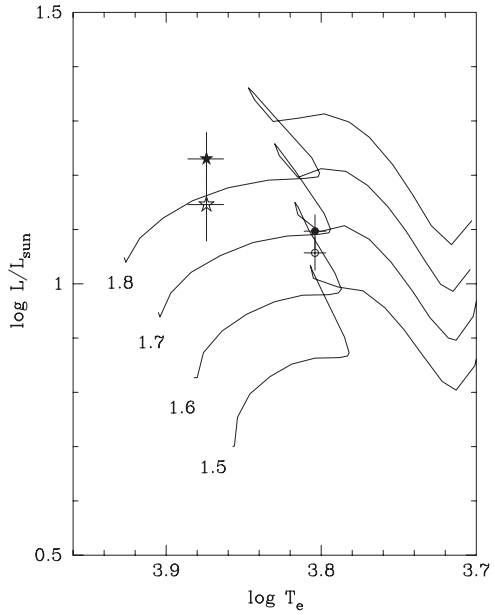

Figure 5. Positions of the components of HR 6979 (stars) and HR 9059 (circles) compared with the 1.5, 1.6, 1.7, and 1.8 $M_\odot$ solar abundance evolutionary tracks of Girardi et al. (2000). The more massive component in each system corresponds to the filled symbol.

those values are 6.60 and 0.341, respectively. With our adopted V mag difference of 0.2, this produces $V = 7.26$ and 7.46 mag for the primary and secondary, respectively. Next, the new reduction of the *Hipparcos* parallax by van Leeuwen (2007) results in a value of 7.59 ± 0.35 mas, which corresponds to a distance of 132 ± 6 pc. Although at such a distance there might be a modest amount of reddening, we have assumed that it is not significant. We then used the individual magnitudes and the revised parallax to obtain absolute magnitudes $M_V = 1.7 \pm 0.1$ mag and $M_V = 1.9 \pm 0.1$ mag for the primary and secondary, respectively. Given the very modest magnitude difference between the components, we adopted the combined $B-V$ color as the color for the individual stars. We then computed a single effective temperature for the components with the formula of Alonso et al. (1996), using an average [Fe/H] value of 0.8 from Stickland (1973). This results in an effective temperature of 7500 K, nearly identical to the value used by Stickland (1973) in his abundance analysis. The bolometric correction for the stars is from Table 3 of Flower (1996). The resulting luminosities of the primary and secondary are $L_1 = 17 \pm 2\ L_\odot$ and $L_2 = 14 \pm 2\ L_\odot$, respectively, while the radii are $R_1 = 2.4 \pm 0.2\ R_\odot$ and $R_2 = 2.2 \pm 0.2\ R_\odot$, respectively. The uncertainties in the computed quantities are dominated by the parallax and the effective temperature uncertainties. The latter is estimated to be ±200 K for the primary and secondary.

Comparison of our estimated effective temperatures and luminosities with evolutionary tracks of Girardi et al. (2000) (Figure 5) indicates that both components are somewhat evolved from the ZAMS, but still within the main-sequence band. The tracks suggest that the actual masses may be about 5% larger than our minimum masses and imply an orbital inclination of about 80°.

7.3. HR 9059

Once again, a determination of the basic properties of the components began with the adoption of the V mag and $B-V$ color of the HR 9059 system, which from the *Hipparcos* catalog (Perryman et al. 1997) are 5.57 and 0.478, respectively. With our assumed V mag difference of 0.1 the apparent V mag of the individual components become 6.27 and 6.37. The new *Hipparcos* parallax reduction by van Leeuwen (2007) results in a value of 14.09 ± 0.36 mas and corresponds to a distance of 71.0 ± 1.8 pc. At this distance, we presumed that interstellar reddening is negligible. We then combined the apparent magnitudes and the parallax to obtain absolute magnitudes $M_V = 2.02 \pm 0.08$ mag and $M_V = 2.12 \pm 0.08$ mag for the primary and secondary, respectively. We next adopted $B-V$ colors of 0.48 for both stars, and then used Table 3 of Flower (1996) to obtain the bolometric corrections and effective temperatures of the two components. The resulting luminosities of the primary and secondary are $L_1 = 12.5 \pm 0.9\ L_\odot$ and $L_2 = 11.4 \pm 0.8\ L_\odot$, respectively, while the radii are $R_1 = 2.9 \pm 0.1\ R_\odot$ and $R_2 = 2.8 \pm 0.1\ R_\odot$, respectively. The uncertainties in the computed quantities are dominated by the parallax uncertainty plus, to a lesser extent, the effective temperature uncertainty, which is estimated to be ±200 K.

We are currently obtaining photometric observations of HR 9059 to determine if there is a second eclipse and also to improve the overall precision of the light curve. A combined spectroscopic and photometric solution of this system, similar to the one computed for HD 71636 (Henry et al. 2006), should significantly improve the basic properties of the components. Nevertheless, it is of interest to compare our estimated basic properties with the evolutionary tracks of Girardi et al. (2000). Figure 5 shows that the two components are at the end of their main-sequence life or perhaps have just begun their short time in the Hertzsprung gap. Thus, they are luminosity class IV–V.

8. CIRCULARIZATION AND SYNCHRONIZATION

The two main theories of orbital circularization and rotational synchronization (e.g., Zahn 1977; Tassoul & Tassoul 1992) disagree significantly on absolute timescales but do agree that synchronization should occur first. Observationally, Matthews & Mathieu (1992) examined 62 spectroscopic binaries with A-type primaries and periods less than 100 days. They concluded that all systems with orbital periods $\lesssim$ 3 days have circular or nearly circular orbits. They also found that many binaries with periods in the range of 3–10 days have circular orbits. Duquennoy & Mayor (1991) examined the multiplicity of solar-type stars in the solar neighborhood. They determined that while systems with periods $\leqslant$10 days had circular orbits, longer period orbits are generally eccentric. All three of our binaries have periods greater than 10 days, so it is not particularly surprising that the systems have eccentric orbits.

In an eccentric orbit, Hut (1981) has shown that the rotational angular velocity of a star will tend to synchronize with that of the orbital motion at periastron. We compute the resulting pseudosynchronous periods with Equation (42) of Hut (1981).

To help in assessing synchronization, we have determined projected rotational velocities from our red-wavelength KPNO spectra with the procedure of Fekel (1997). For A-type stars, the measured line broadening was converted to a $v \sin i$ value. For F-type stars, macroturbulent broadening has been taken into account. Following Fekel (1997), for mid-F stars a value of 4 km s^{-1} was used. To convert the $v \sin i$ values into equatorial rotational velocities, we assume, as is generally done, that the axes of the orbital and rotational planes are parallel, so the inclinations are equal.

8.1. 66 And

To answer the question of whether the components of 66 And are synchronously rotating, we compare our observed velocities with the predicted pseudosynchronous velocities. For 66 And, our $v \sin i$ values, averaged from eight spectra, are 4.2 ± 1.0 and 4.4 ± 1.0 km s^{-1} for the primary and secondary, respectively. The minimum masses of the two components are relatively small. If from Gray (1992) we adopt a mass of 1.38 $M_{\odot}$ for the F4 dwarf primary, combined with its $m \sin^3 i$ value, an orbital inclination of 44° results. If the value of the rotational inclination is the same as that of the orbit, the observed equatorial rotational velocities of both components are 6 km s^{-1}.

The pseudosynchronous rotation period is 9.0 days. This value plus our computed radii from the Stefan–Boltzmann law produce pseudosynchronous rotational velocities of 9 and 8 km s^{-1} for the primary and secondary, respectively. Thus, both stars are rotating more slowly than their pseudosynchronous values.

8.2. HR 6979

For HR 6979, our $v \sin i$ values, averaged from 20 spectra, are 9.1 ± 1.0 and 9.3 ± 1.0 km s^{-1} for the primary and secondary, respectively. Combining the pseudosynchronous rotation period (Hut 1981) of 9.22 days and our computed radii, we obtain pseudosynchronous rotational velocities of 13.2 and 12.1 km s^{-1} for the primary and secondary, respectively. These values are substantially larger than our projected rotational velocities. Indeed, a rotational inclination of about 45° is required to produce the predicted pseudosynchronous rotational velocities. However, the large minimum masses of HR 6979, 1.8 and 1.7 $M_{\odot}$, suggest that the orbital inclination is not far from 90°. Thus, if the orbital and rotational axes are aligned, the measured $v \sin i$ values are very nearly the equatorial rotational velocities. This argues that both components are rotating more slowly than pseudosynchronous.

8.3. HR 9059

For HR 9059, our $v \sin i$ values, averaged from 17 spectra, are 11.5 ± 1.0 and 9.0 ± 1.0 km s^{-1} for the primary and secondary, respectively. The components' minimum masses of 1.6 $M_{\odot}$ are rather large for the adopted spectral types and argue that the orbital inclination is not far from 90°. This conclusion is confirmed by the *Hipparcos* photometry (Perryman et al. 1997), which shows that HR 9059 is an eclipsing binary (Figure 4). Thus, if the orbital and rotational axes are aligned, the measured $v \sin i$ values are very nearly the equatorial rotational velocities. Combining the pseudosynchronous rotation period (Hut 1981) of 7.57 days and our computed radii, we obtain pseudosynchronous rotational velocities of 19.4 and 18.7 km s^{-1} for the primary and secondary, respectively. These values are substantially larger than our projected rotational velocities. This argues that both components are rotating more slowly than pseudosynchronous.

9. CONCLUSIONS

We have determined new, precise spectroscopic orbits for the bright double-lined spectroscopic binaries 66 And, HR 6979, and HR 9059. In particular, the uncertainties of the six minimum masses are all less than 0.2%. We confirm the assessment of Batten et al. (1978) that the orbital period of Northcott is correct. For HR 6979, we have computed an eccentricity that is 50% larger than that found previously. Although this value results in a decrease of nearly 0.2 $M_{\odot}$ in the minimum masses, they are still rather large, indicating that the orbital inclination is close to 90°. However, we found no evidence of eclipses in its *Hipparcos* photometry. The components of HR 9059 also have large minimum masses, suggesting that this system is eclipsing. In this case, analysis of the *Hipparcos* photometry shows that HR 9059 is indeed an eclipsing binary.

We have estimated spectral types of F4 dwarf and F5 dwarf for the components of 66 And. Both components of HR 6979 are Am stars that are still on the main sequence. The components of HR 9059 have spectral classes of F5. Comparison with evolutionary tracks indicates that both stars are at the blue hook end of their main-sequence lifetimes and probably have begun shell helium burning. Thus, the components are about to traverse the Hertzsprung gap or perhaps have just begun this phase of their evolution.

All six components of the three binary systems are rotating more slowly than their predicted pseudosynchronous rotational velocities. In the case of HR 9059, whose components have the largest radii, the observed velocities are roughly 50% less than the predicted pseudosynchronous values.

Using Kepler's third law, Halbwachs (1981) estimated angular separations for over 950 spectroscopic binary systems listed in Batten et al. (1978). For 66 And, HR 6979, and HR 9059 he obtained separations of 2.2, 1.1, and 3.9 mas, respectively. More recently, Taylor et al. (2003) compiled a list of roughly 2000 spectroscopic binaries and determined minimum values of their expected separations by estimating the greater nodal separation for each binary. For 66 And, HR 6979, and HR 9059, their values are 1.87, 1.5, and 2.92 mas, respectively. The two different angular estimates for each of the three binaries are reasonably consistent. Although the separations are small, they are within the scope of modern optical interferometers. Thus, when our spectroscopic results are complemented with high quality interferometric results, accurate three-dimensional orbits, masses, and distances for the systems will follow.

We thank David Doss for his patient guidance, which was essential for the successful operation of the 2.1 m telescope at McDonald and its instrumentation, and Daryl Willmarth for his support of the KPNO coudé feed observations. The research at Tennessee State University was supported in part by NASA grant NCC5-511 and NSF grant HRD-9706268.

REFERENCES

Abt, H. A. 1970, ApJS, 19, 387
Abt, H. A. 1975, ApJ, 195, 405
Abt, H. A., & Bidelman, W. 1969, ApJ, 158, 1091
Abt, H. A., & Levy, S. G. 1969, PASP, 81, 280
Abt, H. A., & Morrell, N. I. 1995, ApJS, 99, 135
Alonso, A., Arribas, S., & Martínez-Roger, C. 1996, A&A, 313, 873
Appenzeller, I. 1967, PASP, 79, 102
Balachandran, S. 1990, ApJ, 354, 310
Barden, S. C. 1985, ApJ, 295, 162
Barker, E. S., Evans, D. S., & Laing, J. D. 1967, R. Obs. Bull., 130, 355
Batten, A. H. 1967, Publ. Dom. Astrophy. Obs., 13, 119
Batten, A. H., Fletcher, J. M., & Mann, P. J. 1978, Publ. Dom. Astrophys. Obs., 15, 121
Bikmaev, I. F., et al. 2002, A&A, 389, 537
Boden, A. F., Torres, G., & Latham, D. W. 2006, ApJ, 644, 1193
Boesgaard, A., & Tripicco, M. 1986, ApJ, 303, 724
Crawford, D. L., Barnes, J. V., Faure, B. Q., Golson, J. C., & Perry, C. L. 1966, AJ, 71, 709
Cowley, A. 1976, PASP, 88, 95
Cowley, A., Cowley, C., Jaschek, M., & Jaschek, C. 1969, AJ, 74, 375

Cunha, M. S. 2007, A&AR, 14, 217
Duquennoy, A., & Mayor, M. 1991, A&A, 248, 485
Eaton, J. A., & Williamson, M. H. 2004, Proc. SPIE, 5496, 710
Eaton, J. A., & Williamson, M. H. 2007, PASP, 119, 886
Fekel, F. C. 1997, PASP, 109, 514
Fekel, F. C., Boden, A. F., Tomkin, J., & Torres, G. 2009a, ApJ, 695, 1527
Fekel, F. C., Tomkin, J., & Williamson, M. H. 2009b, AJ, 137, 3900
Flower, P. J. 1996, ApJ, 469, 355
Girardi, L., Bressan, A., Bertelli, G., & Chiosi, C. 2000, A&AS, 141, 371
Gray, D. F. 1992, The Observation and Analysis of Stellar Photospheres (Cambridge: Cambridge Univ. Press)
Griffin, R. F., & Suchkov, A. A. 2003, ApJS, 147, 103
Halbwachs, J. L. 1981, A&AS, 44, 47
Harper, W. E. 1923, Publ. Dom. Astrophys. Obs., 2, 263
Harper, W. E. 1935, Publ. Dom. Astrophys. Obs., 6, 252
Heard, J. F. 1956, AJ, 61, 318
Heard, J. F. 1958, MNRAS, 118, 341
Henry, G. W., Fekel, F. C., Sowell, J. R., & Gearhart, J. S. 2006, AJ, 132, 2489
Hoffleit, D. 1982, The Bright Star Catalogue (New Haven, CT: Yale Univ. Obs.)
Huenemoerder, D. P., & Barden, S. C. 1984, BAAS, 16, 510
Hummel, C. A., et al. 2001, AJ, 121, 1623
Hut, P. 1981, A&A, 99, 126
Imbert, M. 1977, A&AS, 29, 407
Johnson, H. L., & Morgan, W. W. 1953, ApJ, 117, 313
Matthews, L. D., & Mathieu, R. D. 1992, in ASP Conf. Ser. 32, Complimentary Approaches to Double and Multiple Star Research, ed. H. A. McAlister & W. I. Hartkopf (San Francisco, CA: ASP), 244
McCarthy, J. A., Sandiford, B. A., Boyd, D., & Booth, J. 1993, PASP, 105, 881
Otero, S. 2006, IBVS, 5699, 1
Perryman, M. A. C., et al. 1997, A&A, 323, L49
Petrie, R. M. 1928, Pub. Dom. Astrophys. Obs., 4, 81
Plaskett, J. S., Harper, W. E., Young, R. K., & Plaskett, H. H. 1920, Publ. Dom. Astrophys. Obs., 1, 163
Pourbaix, D., et al. 2004, A&A, 424, 727
Quirrenbach, A. 2001, ARA&A , 39, 353
Scarfe, C. D., Batten, A. H., & Fletcher, J. M. 1990, Publ. Dom. Astrophys. Obs., 18, 21
Slettebak, A. 1955, ApJ, 121, 653
Stickland, D. J. 1973, MNRAS, 161, 193
Strassmeier, K. G., & Fekel, F. C. 1990, A&A, 230, 389
Tassoul, J.-L., & Tassoul, M. 1992, ApJ, 395, 259
Taylor, B. J. 2005, ApJS, 161, 444
Taylor, S. F., Harvin, J. A., & McAlister, H. A. 2003, PASP, 115, 609
Tomkin, J., & Fekel, F. C. 2006, AJ, 131, 2652
Tomkin, J., & Fekel, F. C. 2008, AJ, 135, 555
Torres, G., Andersen, J., & Giménez, A. 2009, A&AR, 18, 67
van Leeuwen, F. 2007, A&A, 474, 653
Wolfe, R. H., Horak, H. G., & Storer, N. W. 1967, in Modern Astrophysics, ed. M. Hack (New York: Gordon & Breach), 251
Yoss, K. M. 1961, ApJ, 134, 809
Young, R. K. 1945, Publ. David Dunlap Obs., 1, 311
Zahn, J.-P. 1977, A&A, 57, 383